ANALES DE MECANICA DE LA FRACTURA VOL. 16 (1999)

THREE-DIMENSIONAL SIMULATION OF DYNAMIC DIAMETRAL COMPRESSION TESTS ON CONCRETE CYLINDERS

G. Ruiz [1], M. Ortiz [2] and A. Pandolfi [3]

[1] Departamento de Ciencia de Materiales, ETSI Caminos, UPM, 28040 Madrid, Spain
[2] Graduate Aeronautical Laboratories, California Institute of Technology, Pasadena, CA 91125, USA
[3] Dipartimento di Ingegneria Strutturale, Politecnico di Milano, 20133 Milano, Italy

Resumen. Este artículo presenta una simulación del comportamiento dinámico del hormigón en tracción. Se trata de una modelización por elementos finitos que permite la aparición de una fisura donde y cuando se alcanza la resistencia a tracción del material. Esto se consigue abriendo la fisura entre los elementos de la malla original y recubriendo la nueva superficie con elementos cohesivos, que son planos y transmiten tensión entre los labios de la fisura en función del valor de su apertura. Este modelo se emplea para reproducir resultados de ensayos de compresión diametral en régimen dinámico obtenidos por medio de una barra Hopkinson. La simulación ajusta bien las cargas transmitidas por la probeta a distintas velocidades de deformación, y reproduce por si misma el patrón de fisuración: predice una serie de fisuras lenticulares paralelas al plano de carga, las cuales se originan en el centro de la cara circular de la probeta y crecen hacia el interior del cilindro y hacia las zonas de carga, y también una multi-fisuración radial secundaria cerca de los apoyos. Estos resultados confirman la valdez de esta técnica numérica para el estudio de procesos de fisuración distribuida en modo mixto en materiales cohesivos, en tres dimensiones y a cualquier velocidad de deformación.

Abstract. This paper presents a simulation of the dynamic response of concrete in tension. It consists of a finite-element modelization that allows the fragmentation of the bulk when and where the static tensile strength of the material is reached. This is done by allowing the opening of a crack between the elements existing in the initial mesh, and tiling the new surface with cohesive elements, i. e. with plane elements able to transmit tension between the crack lips as a function of the crack opening. This model is checked using some detailed results of dynamic brazilian tests obtained by means of a Hopkinson bar. The simulation gives accurate transmitted loads for different strain rates, and accounts by itself for the crack pattern: it predicts a series of main principal lens-shaped cracks parallel to the load plane, that initiate in the center of the circular surface and grow towards the interior of the cylinder and the bearing strips, as well as a secondary radial multi-cracking near the supports. These results validate this numerical procedure for studying mixed-mode multi-cracking processes in cohesive materials in 3-D at any strain-rate.

1 INTRODUCTION

In this paper we investigate the feasibility of using cohesive theories of fracture, in conjunction with the direct simulation of fracture and fragmentation, in order to describe processes of tensile damage and compressive crushing in concrete specimens subjected to dynamic loading. We account explicitly for microcracking, the development of macroscopic cracks and inertia, and the effective dynamic behavior of the material is *predicted* as an outcome of the calculations. Indeed, the cohesive properties of the material are assumed to be rate-independent, and are therefore determined by static properties such as the static tensile strength. The ability of model to predict key aspects of the dynamic behavior of concrete, such as the strain-rate sensitivity of strength may be traced to the fact that cohesive theories, in addition to building a characteristic length into the material description, they endow the material with an intrinsic *time scale* as well [1]. This intrinsic time scale permits the material to discriminate between slow and fast loading rates and ultimately allows for the accurate prediction of the dynamic strength of the material as a function of strain rate and other rate effects.

The particular configuration contemplated in this study is the brazilian cylinder test performed in a split-Hopkinson pressure bar (SHPB). Our simulations give accurate transmitted loads over a range of strain rates, which attests to the fidelity of the model where rate effects are concerned. The model also predicts key features of the fracture pattern such as the primary lens-shaped cracks parallel to the load plane, as well as the secondary profuse cracking near the supports. The primary cracks are predicted to be nucleated at the center of the circular bases of the cylinder

and to subsequently propagate towards the interior, in accordance with experimental observations. These results validate the theory as it bears on mixed-mode fracture and fragmentation processes in concrete over a range of strain rates.

Next section briefly describes the fundamentals of the cohesive elements and its implementation into a general FE code, and section 3 explains the basic features of the experimental set-up, that is intended to get the tensile strength of concrete at high strain-rates (§3.1). Next follows a description of the simulation, comprising the specimen geometry and material parameters (§3.2), the load and boundary conditions (§3.3), the mesh used throughout the runs (§3.4) and the numerical results compared to the experimental ones (§3.5). Finally section 4 draws some conclusions.

2 FINITE ELEMENT MODEL

We start by considering a deformable body undergoing a motion described by a deformation mapping $\bar{\varphi}$ and containing a collection of cohesive cracks. The locus of these cracks on the undeformed configuration is denoted S_0, and its unit normal $\bar{n}$. The jump of $\bar{\varphi}$ across S_0 defines the opening displacement $\bar{\delta}$.

Following Camacho and Ortiz [1] and others [2, 3], we consider a simple class of mixed-mode cohesive laws accounting for tension-shear coupling obtained by the introduction of an effective opening displacement:

$$\delta = \sqrt{\beta^2 \delta_S^2 + \delta_n^2} \tag{1}$$

where

$$\delta_n = \bar{\delta} \cdot \bar{n} \tag{2}$$

is the normal opening displacement and

$$\delta_S = |\bar{\delta}_S| = |\bar{\delta} - \delta_n \bar{n}| \tag{3}$$

is the magnitude of the sliding displacement. The parameter β assigns different weights to the sliding and normal opening displacements. The cohesive law relates δ to a scalar effective traction, which expression is:

$$t = \sqrt{\beta^{-2} |\bar{t}_S|^2 + t_n^2} \tag{4}$$

where $\bar{t}_S$ and t_n are the shear and the normal traction respectively. From this relation, we observe that β defines the ratio between the shear and the normal critical tractions.

Upon closure, the cohesive surfaces are subjected to the contact unilateral constraint, including friction. We regard contact and friction as independent phenomena to be modelled outside the cohesive law. Friction may significantly increase the sliding resistance in closed cohesive surfaces. In particular, the presence of friction may result in a steady –or even increasing– frictional resistance while the normal cohesive strength simultaneously weakens.

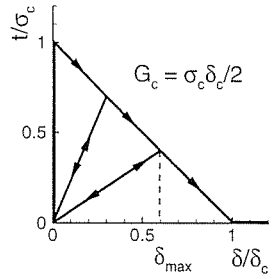

Figure 1: Linear irreversible cohesive law.

We assume the existence of a loading envelop defining a relation between t and δ under conditions of loading. A simple and convenient relation is furnished by the linearly decreasing envelop shown in Fig. 1. Following Camacho and Ortiz [1] we shall assume unloading to the origin, Fig. 1, giving

$$t = \frac{t_{\max}}{\delta_{\max}} \delta, \qquad \text{if} \qquad \delta < \delta_{\max} \text{ or } \dot{\delta} < 0 \tag{5}$$

It is a well-known fact [4] that cohesive theories introduce a well-defined length scale into the material description and, in consequence, are sensitive to the size of the specimen. Camacho and Ortiz [1] have noted that in conjunction with inertia cohesive models introduce a *characteristic time* as well. Owing to this intrinsic time scale, the material behaves differently when subjected to fast and slow loading rates. The calculations presented subsequently demonstrate the ability of cohesive theories to account for the dynamic strength of brittle solids, i. e., the dependence of the dynamic strength on strain rate.

An appealing aspect of cohesive laws as models of fracture is that they fit naturally within the conventional framework of finite element analysis. We follow Camacho and Ortiz [1] and adaptively create new surfaces as required by the cohesive model by duplicating nodes along previously coherent element boundaries. The nodes are subsequently released in accordance with a tension-shear cohesive law. The particular class of cohesive elements used in calculations has been developed by Ortiz and Pandolfi [3] and consists of two six-node triangles endowed with quadratic displacement interpolation, Fig. 2.

Formulating the virtual work principle for the body and inserting the displacement interpolation into it leads to a system of semi-discrete equations of motion of the form:

$$\bar{M}\ddot{\bar{x}} + \bar{f}^{\text{int}}(\bar{x}) = \bar{f}^{\text{ext}}(t) \tag{6}$$

where $\bar{x}$ is the array of nodal coordinates, $\bar{M}$ is the mass matrix, $\bar{f}^{\text{ext}}$ is the external force array, and $\bar{f}^{\text{int}}$ is the internal force array. In calculations we use the second-order

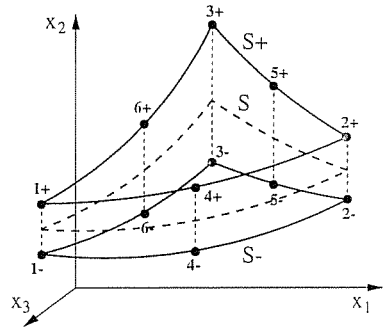

Figure 2: Geometry of cohesive element. The surfaces S^- and S^+ coincide in the reference configuration of the solid.

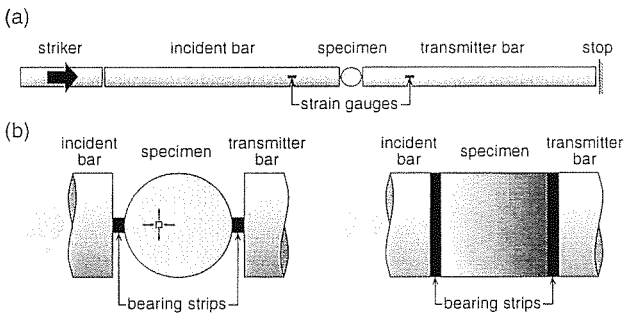

Figure 3: Experimental set-up (a), and detail of the specimen (b).

accurate central difference algorithm to discretize (6) in time [5].

3 SIMULATION OF THE DYNAMIC BEHAVIOR OF CONCRETE

3.1 Experimental set-up

The SHPB consists of an incident bar and a transmitter bar, with a short specimen placed between them, and a striker bar that impacts the incident bar to produce a longitudinal compressive pulse that propagates toward the specimen (Fig. 3a). The pulse is partially reflected in the border of the incident bar, and partially transmitted through the specimen. In this case the diametral loading generates tension perpendicular to the load plane (Fig. 3b), which eventually causes the specimen to split.

The strain records corresponding to the incident, reflected and transmitted pulses are used to calculate the corresponding stress pulses and the dynamic splitting tensile stress, f'_{td}, which derives from the following equation:

$$f'_{td} = \frac{2P_T}{\pi W D} \tag{7}$$

where P_T is the maximum load transmitted through the cylinder and W and D are respectively the width and diameter of the cylinder. P_T is calculated from the maximum transmitted stress, σ_T, as:

$$P_T = \pi R^2 \sigma_T \tag{8}$$

The strain rate can de determined from the next equation:

$$\dot{\epsilon} = \frac{f'_{td}}{E\tau} \tag{9}$$

where E is the concrete elastic modulus and τ is the time delay between the start and the peak of the transmitted pulse.

Density, $\rho =$	2405	kg/m^3
Elastic modulus, $E =$	37.9	GPa
Static direct tensile strength, $f_{ts} =$	4.53	MPa
Fracture energy, $G_c =$	66.2	N/m
Characteristic length, $EG_c/f_{ts}^2 =$	122	mm
Characteristic time, $\rho c \delta_c / 2 f_{ts} =$	31	μs

Table 1: Concrete parameters

3.2 Specimen geometry and material parameters

The simulations in this paper refer to experiments reported by Hughes, Tedesco and Ross [7], Tedesco, Ross and Kuennen [6] and Ross, Tedesco and Kuennen [8]. The specimens are concrete cylinders of 50.8 mm diameter and height obtained by coring from a concrete block. The maximum aggregate size is 8.5 mm, and the material parameters are listed in Table 1. All of them were obtained by independent tests except the fracture energy, that is estimated here following the recommendation established in the Model Code [9]. The cohesive law is supposed to be linear-irreversible and is depicted in Fig. 1.

There is experimental evidence [10, 11] which suggests that the intrinsic fracture toughness of concrete, i. e., the critical stress intensity factor required to advance a semi-infinite crack within its plane in the absence of kinking, is much larger in pure mode II that in pure mode I owing to the interlocking of aggregate particles. This in turn suggests adopting a large value of the coupling parameter β in (1), since, as remarked earlier, β gives the ratio of mode II to mode I fracture toughness. Based on a suggestion by Gustafsson and Hillerborg [12] on the relative strengths of concrete in tension and shear, in calculations we take $\beta = 10$. Under the assumptions just stated, a semi-infinite crack subjected to mixed-mode loading will tend to kink at an angle roughly corresponding to the maximum circumferential stress in its K-field. Indeed, the maximum circumferential stress criterion is known to lead to accurate predictions of crack paths in concrete [13].

3.3 Load and boundary conditions

The tests were performed at different load levels leading to several strain rates. The loading pulse can be simplified

Load case No.	Rise time t_r (μs)	Stress level σ_i (MPa)	Related velocity v (m/s)
1	66	60.2	1.5
2	72	72.8	1.8
3	80	79.4	2.0
4	85	122.5	3.1
5	41	184.5	4.7
6	48	264.3	6.7

Table 2: Parameters for the incident load pulses

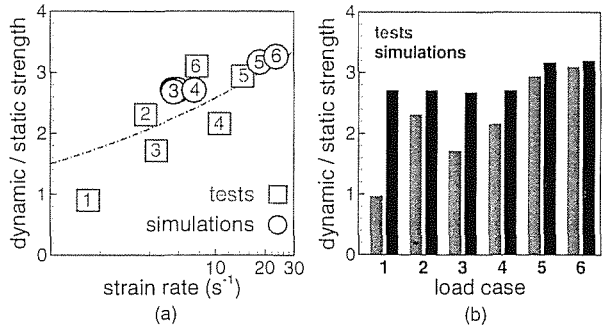

Figure 4: Comparison of experimental and numerical rate-sensitivity curves and dynamic strength of concrete.

to a linear rise followed by a plateau and the rise time and stress level corresponding to each one of the load cases are given in Table 2. The incident stress σ_i can be directly related to the velocity of the incident bar cross section, v, by simplifying the impact with the striker to that of a moving rigid body impacting a stationary bar [14], which gives $v = \sigma/\rho c$, where ρ and c are the density and the one-dimensional wave velocity of the incident bar.

3.4 Mesh used in the simulation

The mesh used in the simulation comprises 8378 nodes and 5669 10-node quadratic tetrahedra, and is designed so as to be fine and nearly uniform on and in the vicinity of the load plane, and to gradually coarsen away from the load plane. The mesh size roughly ranges from 1/15 to 1/30 of the characteristic cohesive length (Table 1) of the material and may, therefore, be expected to yield objective and mesh-size insensitive results [1].

3.5 Simulation results

Selected results of the calculations and comparisons with experimental data are shown in Figs. 4, and 5. The main features of these results, as regards load histories, dynamic strength and crack patterns, are next discussed in turn.

Dynamic strength and rate sensitivity
Fig. 4 compares the predicted and observed ratio of static to dynamic strengths for all loading cases under consideration, and the dependence of the dynamic strength on strain rate. In addition, the curve inset in Fig. 4a represents a linear fit to the experimentally observed strain-rate dependence of the dynamic strength. As may be seen from Fig. 4a, the calculations capture well the overall rate-sensitivity of the material, which takes the form of a steady rise in dynamic strength with increasing strain rate. It is interesting to note that the simulations corresponding to loading cases 1, 2 and 3 yield comparable results, Fig. 4a, which may be due to the compensating effect of a simulataneous increase in rise time and impact velocity in the load pulse (cf Table 2). The accuracy in the calculation of the peak transmitted load and, by extension, of the dynamic strength, Eq. (7), is equally satisfactory, with the exception of loading case 1, Fig. 4b. Note that the dynamic strength reported for this case is below the static strength, which constitutes a clear experimental anomaly.

Load and energy history curves
A comparison between computed and experimental load-histories for loading case 2 is shown in Fig. 5. The two histories match nearly exactly during the early stages of loading. The discrepancy in the peak loads, of the order of 17%, and in the slope of the ramp portion of the record are well within the experimental scatter. The horizontal dash line inset in Fig. 5a represents the maximum load attained during the static Brazilian test and is shown for reference. As may be seen from the figure, the dynamic peak load is of the order of 3 times the static maximum load, which attests to the importance of the dynamic effects under the conditions of the test.
Fig. 5 also depicts the consumption of cohesive energy and the kinetic energy as a function of time for the same loading case. The horizontal dash line shown for reference represents the fracture energy expended in the formation of a single planar crack cutting through the midplane of the specimen. As may be observed, the actual fracture energy expended is greatly in excess of that value, which is indicative of a far more complex and intricate crack pattern. On the other hand, the increase in kinetic energy that accompanies the loss of load-carrying capacity points out that a widespread dynamic fragmentation takes place after the load peak.

Crack pattern
The predicted sequence of crack patterns also follows closely the experimental patterns observed by means of a high speed camera [6] (see inset in Fig. 5) . Fig. 5 also depicts a sequence of snapshots of the deformed specimens at intervals of 10 μs, showing the distribution of cracks. It should be carefully noted that, in this plots, displacements have been magnified by a factor of 100 in order to aid visualization. It may also be recalled that the peak load occurs roughly at 70 μs, corresponding to snapshot Fig. 5f. Also shown in the figures are level contours of damage, defined as the fraction of expended fracture energy to total fracture energy per unit surface, or critical energy release rate. Thus, a damage density of zero de-

notes an uncracked surface, whereas a damage density of one is indicative of a fully cracked or free surface. It bears emphasis that this damage field is defined on any internal surface of the body, i. e., it represents a density per unit area–as opposed to a a density per unit volume. In Fig. 5 we have chosen to represent the extent of damage on the midplane, or load plane, of the specimen.

Remarkably, both the experimental observations and the numerical solution clearly exhibit a main crack on the midplane of the specimen which initiates near the center of the cylinder and subsequently propagates towards the bearing strips, eventually causing the specimen to split into two main fragments. The observed initiation time is roughly 30 μs, which is in fair agreement with the results of the calculations, Figs. 5b and c. Furthermore, the simulation also captures some early localized cracking in the loading area, Fig. 5b. The initiation and growth of the main crack is far from being uniform through the width of the specimen. Indeed, our simulations suggest that lenticular cracks initiate from the surface of the specimen, i. e., the ends of the cylinder, Figs. 5c and d, and subsequently propagate inward within the midplane with increasing load. Eventually, the surface cracks coalesce and form a single through-crack, Figs. 5d-f.

4 SUMMARY AND CONCLUSIONS

We have investigated the feasibility of using cohesive theories of fracture, in conjunction with the direct simulation of fracture and fragmentation, in order to describe processes of tensile damage and compressive crushing in concrete specimens subjected to dynamic loading. The particular configuration contemplated in this study is the brazilian cylinder test performed in a Hopkinson bar, which furnishes a demanding validation test of the theory. Our approach accounts explicitly for microcracking, the development of macroscopic cracks and inertia. The effective dynamic behavior of the material is *predicted* as an outcome of the calculations. In particular, our simulations capture closely the experimentally observed rate-sensitivity of the dynamic strength of concrete, i. e., the nearly linear increase in dynamic strength with strain-rate. More generally, our simulations give accurate transmitted loads over a range of strain rates, which attests to the fidelity of the model where rate effects are concerned. The model also predicts key features of the fracture pattern such as the primary lens-shaped cracks parallel to the load plane, as well as the secondary profuse cracking near the supports. These results validate the theory as it bears on mixed-mode fracture and fragmentation processes in concrete over a range of strain rates.

We have assumed that the cohesive properties of the material are rate-independent and therefore determined by static properties such as the static tensile strength. However, we have noted that cohesive theories, in addition to building a characteristic length into the material description, endow the material with an intrinsic *time scale* as well. This intrinsic time scale accounts for the ability of model to predict key aspects of the dynamic behavior of concrete, such as the strain-rate sensitivity of strength. Our results suggest, therefore, that most of the strain rate-sensitivity of concrete is attributable to the microinertia attendant to dynamic microcracking and fracture. We have also found that the cohesive energy expenditure is considerably larger in the dynamic test than in the static case, which reflects the dissipation due to microcracking.

5 ACKNOWLEDGEMENTS

Gonzalo Ruiz gratefully acknowledges the financial support for his stay at the *California Institute of Technology* provided by the *Dirección General de Enseñanza Superior, Ministerio de Educación y Cultura*, Spain. Anna Pandolfi and Michael Ortiz are grateful for support from the Department of Energy through Caltech's ASCI Center of Excellence for Simulating Dynamic Response of Materials. Michael Ortiz also wishes to gratefully acknowledge the support of the Army Research Office through grant DAAH04-96-1-0056. We are indebted to Dr. Raúl A. Radovitzky for his assistance in the development of the meshes used throughout this research.

References

[1] Camacho, G. T. and Ortiz, M., "Computational Modelling of Impact Damage in Brittle Materials", *International Journal of Solids and Structures*, Vol. 33 (20-22), pp. 2899–2938, (1996).

[2] De-Andrés, A., Pérez, J. L. and Ortiz, M., "Elastoplastic Finite Element Analysis of Three-Dimensional Fatigue Crack Growth in Aluminum Shafts Subjected to Axial Loading", *International Journal of Solids and Structures*, in press.

[3] Ortiz, M. and Pandolfi, A., "A Class of Cohesive Elements for the Simulation of Three-Dimensional Crack Propagation", *International Journal for Numerical Methods in Engineering*, (1998).

[4] Bažant Z. P. and Planas J., " Fracture and Size Effect in Concrete and other Quasibrittle Materials", CRC Press, Boca Raton, Florida (1998).

[5] Hughes, T. J. R., "Analysis of Transient Algorithms with Particular Reference to Stability Behavior", in *Computational Methods for Transient Analysis*, T. Belytschko and T. J. R. Hughes Eds., North-Holland, pp. 67–155 (1983).

[6] Tedesco, J. W., Ross, C. A. and Kuennen, S. T., "Experimental and Numerical Analysis of High-Strain

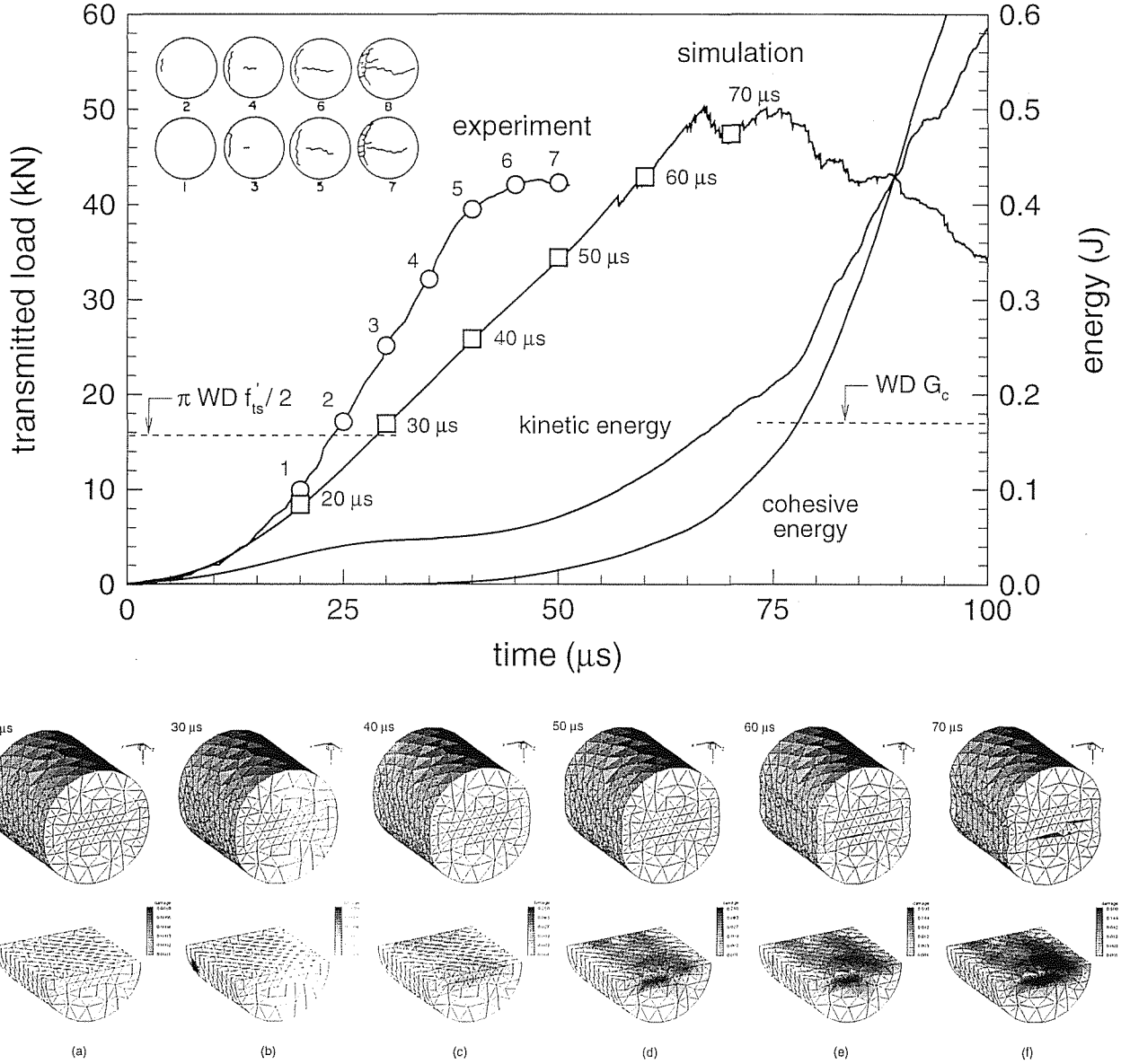

Figure 5: Comparison of experimental and numerical results for loading case 2.

Rate Splitting Tensile Tests", *ACI Materials Journal*, Vol. 90 N. 2, pp. 162–169, (1993).

[7] Hughes, M. L., Tedesco, J. W. and Ross, A., "Numerical Analysis of High Strain Rate Splitting-Tensile Tests", *Computers and Structures*, Vol. 47, pp. 653–671(1993).

[8] Ross, A., Tedesco, J. W. and Kuennen, S. T., "Effects of Strain Rate on Concrete Strength" *ACI Materials Journal*, Vol. 92, pp. 37–47, (1995).

[9] CEB-FIP Model Code 1990, Final Draft, CEB-FIP, *Bulletin D'Information N. 203, 204 and 205*, EFP Lausanne, (1991).

[10] Jia, Z., Castro-Montero, A. and Shah, S. P., "Observation of Mixed Mode Fracture with Center Notched Disk Specimens", *Concrete and Cement Research*, Vol. 26, pp. 125–137, (1996).

[11] Subrumaniam, K.V., Popovics, J.S. and Shah, S.P., "Testing Concrete in Torsion: Instability Analysis and Experiments", *Journal of Engineering Mechanics, ASCE*, Vol. 124 N. 11, pp. 1258–1268, (1998).

[12] Gustafsson, P.J. and Hillerborg, A., "Sensitivity in the Shear Strength of Longitudinally Reinforced Beams to Fracture Energy of Concrete", *ACI Structural Journal*, Vol. 85 N. 3, pp. 286–294, (1988).

[13] Gálvez, J. C., Cendón, D., Planas, J., Guinea, G. V. and Elices, M., "Fracture of Concrete Under Mixed Loading. Experimental Results and Numerical Prediction", in *Fracture Mechanics of Concrete Structures*, Proceedings Framcos-3, Aedificatio Publishers, D-79104, Freiburg, Germany, (1998).

[14] Nicholas, T. and Recht, R. F., "Introduction to Impact Phenomena", in *High Velocity Impact Dynamics*, Zukas, J. A. Ed., John Wiley and Sons, pp. 1–63 (1990).